RSC Advances

PAPER

View Article Online
View Journal | View Issue

Cite this: *RSC Adv.*, 2025, **15**, 3066

Removal of active pharmaceutical compounds in Primalan and Diane using pumpkin biochar: synthesis, characterization, and adsorption study

Boudoumi Barkahoum,[ab] Guergazi Saadia *[ab] and Nouioua Asma[bc]

This investigation aims to apply the adsorption process to eliminate mequitazine and ethinylestradiol, the active molecules of Primalan and Diane, respectively, from aqueous solutions, utilizing biochar synthesized from pumpkin fruits (PB-500). The results revealed that the obtained adsorbent possessed a notable specific surface area, contributing to removal efficiencies of 66.61% and 62.37% for mequitazine and ethinylestradiol, respectively. The sludge recovered under equilibrium conditions was also characterized to facilitate comparison of biochar properties before and after adsorption. Several models were employed to analyze the adsorption kinetics and isotherms, showing that the pseudo-second-order model offers the optimal representation for the kinetic behavior. Both the Sips and Freundlich models accurately described the isotherm data. On the other hand, the adsorption on PB-500 was clearly affected by the variation in solution pH. The PB-500 variation test indicated that the optimum adsorbent concentration was around 0.8 g L^{-1}, where the removal yields were 67% for mequitazine and 65.16% for ethinylestradiol. Thermodynamic studies indicated that the adsorption was exothermic for both pollutants. Consequently, it can be inferred that pumpkin-biochar serves as an effective adsorbent for eliminating mequitazine and ethinylestradiol from water.

Received 6th November 2024
Accepted 26th December 2024

DOI: 10.1039/d4ra07917e

rsc.li/rsc-advances

1. Introduction

Over the recent decades, advancements in medicine have led to a significant increase in the production and consumption of pharmaceutical products, with approximately 3000 distinct products and annual production volumes surpassing hundreds of tons.[1] Among the widely consumed medications are mequitazine and ethinylestradiol. The former is used to relieve various allergy rhinitis symptoms, which affects 40% of the word population, presenting continuous increase over the last 20 years.[2] The latter is a hormonal treatment, a derivative of progesterone, used as a hormonal contraceptive and for acne treatment. The oral contraceptive pill is the most popular method of contraception, with the worldwide consumption surpassing 100 million.[3] The extensive utilization of pharmaceuticals in healthcare has led to the release of significant amounts of these compounds into the environment, in both unutilized and metabolized forms.[4,5] These active compounds, such as antibiotics, antiepileptics, hormones, and analgesics, have been classified as emerging contaminants. They are characterized by their low concentrations (nanograms or micrograms per liter) but also by their potential impact on aquatic ecosystems and human health.[6–8] Conventional wastewater treatment methods are the common source of pharmaceutical compounds in discharged effluents.[9] Traditional treatment processes typically fail to achieve complete neutralization of the toxic compounds present in wastewater[10] due to factors such as their chemical structure, concentrations, solubility, charge and their ability to escape several purification steps.[11,12] The accumulation and discharge of effluents containing pharmaceuticals and personal care products into water bodies can induce genotoxic, mutagenic, and ecotoxicological effects on plants, animals, and human health. The continuous release of these contaminants into water bodies and their subsequent exposure may potentially lead to chronic, long-term consequences for aquatic plants and animals.[13]

Multiple treatment techniques are employed to confront the challenge of removing pharmaceuticals and emerging organic contaminants from water, including adsorption, reverse osmosis, aerobic and anaerobic digestion, ozonation, Fenton and other advanced oxidation processes.[14] Adsorption technologies stand out as a popular method because of their adaptability, simplicity, and effectiveness,[15–17] as well as their ability to avoid producing harmful by-products, unlike advanced oxidation and membrane techniques.[18] The effectiveness of adsorption depends directly on the choice of material employed as the adsorbent.[19,20] A biochar-originated by-product of biomass pyrolysis has been investigated as a promising cost-effective

[a]*Civil Engineering and Hydraulic Department, University of Biskra, PO Box 145 RP, Biskra, Algeria. E-mail: s.guergazi@univ-biskra.dz*

[b]*Research Laboratory in Subterranean and Surface Hydraulics, University of Biskra, PO Box 145 RP, Biskra, Algeria*

[c]*Department of Industrial Chemistry Faculty of Science and Technology, University of Biskra, Algeria*

adsorbent for eliminating pharmaceuticals from aqueous solutions[21,22] due to its abundance of functional groups,[23] porous structure, rich aromatic compounds, and environmentally friendly characteristics.[24,25] Biochars derived from agricultural or plant residues at low cost have been demonstrated to exhibit an effective adsorption performance.[25,26]

Pharmaceutical contamination in aquatic environments has drawn increasing attention due to its ecological and health impacts. Despite extensive studies on pharmaceutical adsorption, the specific pharmaceuticals investigated in this research (mequitazine and ethinylestradiol) remain limited. This research gap highlights the novelty and relevance of this study.

Therefore, the aim of this study was to apply the adsorption process for the removal of mequitazine and ethinylestradiol from aqueous solutions, using a biochar synthesized from pumpkin peels. It is crucial to point out that the removal of mequitazine and ethinylestradiol was investigated by studying the case of the commercial pharmaceuticals Primalan and Diane, respectively. The prepared biochar was characterized using multiple analyses: Fourier transform infrared (FTIR) spectroscopy, X-ray diffraction (XRD), scanning electron microscopy (SEM), energy-dispersive X-ray spectroscopy (EDX) for the determination of elemental composition, Brunauer–Emmett–Teller (BET) method and pH of zero charge point (pH_{pzc}), and PB-500 was also characterized after adsorption to completely understand the mechanism. It is worth mentioning that the biochar used in this study has inherent limitations, as it is typical for non-activated biochars. However, the research primarily aimed to evaluate the potential of an unmodified, low-cost adsorbent derived from agricultural residues. Although activation could significantly enhance the surface area and adsorption efficiency, this aspect is beyond the scope of the present work. Different parameters such as contact time, pH medium, adsorption isotherm, adsorbent dosage and thermodynamics were analysed in order to optimize the process efficiency. Different linear and nonlinear models were investigated to analyze the experimental results of kinetic and isotherm studies. The obtained results show the alignment and the accuracy of mequitazine and ethinylestradiol elimination compared with those obtained from other compounds with similar compositions, representing remarkable removal efficiency.

2. Material and methods

2.1. Solution preparation

The employed pharmaceuticals, namely Primalan (5 mg of mequitazine) and Diane (35 μg of ethinylestradiol), were procured as tablets from Pierre Fabre and Bayer AG, respectively. Mequitazine and ethinylestradiol exhibit distinct chemical and physical properties, which are listed in Table 1. The stock solutions were prepared at concentrations of 120 mg L^{-1} for mequitazine and 81.4 mg L^{-1} for ethinylestradiol. To achieve these concentrations, a known quantity of tablets was dissolved in distilled water. These stock solutions were periodically prepared to ensure consistency throughout the study, providing the requisite concentrations for subsequent experiments.

Table 1 Physicochemical properties of the monitored substances

Properties	Mequitazine	Ethinylestradiol
Chemical structure	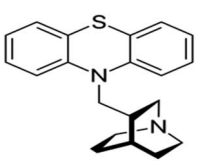	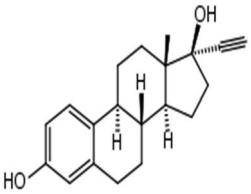
Molecular formula	$C_{20}H_{22}N_2S$	$C_{20}H_{24}O_2$
Molecular weight	322.47 g mol^{-1}	296.4 g mol^{-1}
pK_a	10.43	10.4
Solubility	0.1 mg ml	4.8 mg L^{-1}
Wave length	256 nm	280 nm

2.2. Preparation of pumpkin biochars

Pumpkin peels were rinsed several times with deionized water, crushed into small pieces and then dried in ambient air. After that, pumpkin samples were placed in a DAIHAN scientific furnace at 500 °C for 1 h under oxygen-limited conditions at a heating rate of 10 °C min^{-1}. After pyrolysis, the obtained material was soaked in 0.05 M of HCl and then washed with distilled water until achieving a pH in the range from 6.5 to 7. The addition of a few drops of hydrochloric acid (HCl) after pyrolysis is generally used to neutralize ashes or basic substances that may have formed during the pyrolysis process. Finally, the PB-500 sample was air-dried in an oven at 80 °C for 24 hours and then crushed. The sample was separated using a 1 mm-mesh metal electronic sieve from KARP MACHINERY to achieve a uniform particle size.

2.3. Characterization

Pumpkin biochar samples were characterized by ultimate analysis. The functional groups on the surface were identified by FTIR (Fourier transform infrared) spectroscopy using an Agilent Cary 630 FTIR spectrometer, in the wavelength range of 400–4000 cm^{-1}. The structure of the biochar was assessed by X-ray diffraction (XRD) using a D8 Advance, while its chemical composition was analyzed by energy-dispersive X-ray spectroscopy (EDX). The EDX analysis was conducted over the entire sample surface to obtain an average composition, ensuring a representative understanding of the elemental distribution. This combined approach provided comprehensive insights into the biochar's structural and surface characteristics, with a particular focus on the overall surface characterization for this study. The morphology was examined using a Thermo Scientific Prisma-E scanning electron microscope (SEM), and the sample was scanned to generate high-resolution images, providing insights into the pore structure and the elemental composition (EDX). The textural characteristics were analyzed from nitrogen adsorption desorption isotherms at 77 K by BET measurement (ASAP 2020). For the pH of point zero charge, Chebbi *et al.*[27] described the protocol used. First, 50 mg of PB-500 was mixed with 50 ml of 0.1 M NaCl and stirred for 24 h at different initial

pH values, which was adjusted using 0.1 M HCl and 0.1 M NaOH. The pH_{pzc} was acquired by achieving zero difference between the initial and the final pH values.

2.4. Adsorption experiments

All experiments were conducted in a batch system at 20 °C. Adsorption tests were conducted in 100 ml beakers containing 50 ml of distilled water with determined doses of pollutants mixed with 0.5 g L^{-1} of PB-500, under agitation of 1000 rpm for a specific time using a magnetic agitator. The solutions were filtered using a vacuum pump with filters of 0.45 μm diameter. The residual concentration was assessed using a photo-Lab*7600 UV-VIS spectrophotometer at a wavelength of 256 nm for mequitazine and 281 for ethinylestradiol.[28,29]

Different parameters, such as stirring time (2–120 min) to define the equilibrium time and pH medium (2–12) to see the efficiency of the adsorption process under normal conditions and under other conditions, adsorption isotherm where the initial concentration of pharmaceuticals was varied (2–20 mg L^{-1}), adsorbent dosage where the PB-500 concentration was changed until it attained the optimal value (0.2–3 g L^{-1}) and the temperature effect (20, 40, 50 °C), were used in this study. The adsorption capacity of PB-500 tested at time t (q_t, mg g^{-1}) and at equilibrium (q_e, mg g^{-1}) was calculated using the following equations:

$$q_t = \frac{(C_0 - C_t) \times V}{m} \quad (1)$$

$$q_e \frac{(C_0 - C_e) \times V}{m} \quad (2)$$

The removal efficiency was estimated as follows:

$$\%\text{Removal} = \frac{C_0 - C_e}{C_0} \times 100 \quad (3)$$

where C_0, C_t, and C_e (mg L^{-1}) are the concentrations of the pollutant initially, at given time and at equilibrium, v (L) is the solution volume and m (g) represents the amount of PB-500 used.

2.5. Adsorption empirical models

Nonlinear fitting models were employed to discuss the kinetic adsorption experiments, including pseudo first-order-order (PFO), pseudo-second-order (PSO), Elovich, Avrami and intra-particle diffusion (linear model). All isotherm adsorption models tested were nonlinear, which were Langmuir, Freundlich, Temkin, Redlich–Peterson, Dubinin–Radushkevich and Sips. Table 2 lists all the kinetic and isotherm models used.

The model performance was analyzed by determining various statistical parameters[30] such as adjusted coefficient (adj-R^2) (eqn (4)) and reduced chi-squared (red-χ^2) (eqn (5)), where adj-R^2 should be close to 1, indicating the fit between the data and the model, while red-χ^2 must approach zero, revealing the discrepancies between the calculated and the experimental values:[31]

Table 2 Kinetic and isotherm analysis models used

Model	Equation	Parameter definition	References
Kinetic models			
Pseudo-first-order (PFO)	$q_t = q_e(1 - e^{-k_1 t})$	k_1 (min^{-1}) and k_2 (g mg^{-1} min^{-1}) are the speed	32
Pseudo-second-order (PSO)	$q_t = \frac{q_e^2 k_2 t}{1 + q_e k_2 t}$	Constants for PFO and PSO, respectively	33
Intra-particle diffusion	$q_t = K_{int} t^{1/2} + C$	C (mg g^{-1}) represents the constant related to the thickness of the boundary layer, K_{int} (mg g^{-1} $min^{-1/2}$) is the rate constant of Weber Morris model	34
Elovich	$q_t = \frac{1}{\beta} \ln(\alpha\beta t + 1)$	α (mg g^{-1} min^{-1}) is the initial adsorption rate constant and β (g mg^{-1}) is the desorption rate constant	35
Avrami	$q_t = q_e(1 - e^{-(K_{AV} \cdot t^{n_{AV}})})$	K_{AV} (min^{-1}) is the Avrami model constant and n_{AV} (dimensionless) is a fractional order of adsorption	36
Isotherm models			
Langmuir	$q_e = \frac{Q_{max} K_L C_e}{1 + K_L C_e}$	Q_{max} (mg g^{-1}) is the maximum adsorption capacity and K_L (L mg^{-1}) is the Langmuir model constant	37
Freundlich	$q_e = K_F C_e^{\frac{1}{n}}$	K_F ((mg g^{-1})/(mg L^{-1})^n) and n (dimensionless) are the Freundlich model constants	38
Temkin	$q_e = A \ln(K_T \cdot C_e)$	A (mg g^{-1}) and K_T (L mg^{-1}) are the Temkin model constants	39
Redlich–Peterson	$q_e = \frac{K_{RP} C_e}{1 + \alpha_{RP} C_e^{\beta}}$	K_{RP} (mg L^{-1})$^{-g}$, α_{RP} (L mg^{-1}) and β (dimensionless) are the Redlich–Peterson model constants	40
Dubinin–Radushkevich	$q_e = q_m \cdot e^{-\beta\varepsilon^2}$	q_m (mg g^{-1}) is the theoretical saturation capacity, β (mol^2 kJ^{-2}) is a coefficient related to the adsorption energy and ε is the Polanyi potential (kJ mol^{-1}), where: $\varepsilon = RT \ln\left(1 + \frac{1}{C_e}\right)$	41
Sips	$q_e = \frac{q_s \times K_S \times C_e^{\frac{1}{n_S}}}{1 + K \times C_e^{\frac{1}{n_S}}}$	q_s (mg g^{-1}) is the maximum adsorption capacity, K_S is the Sips model constant and n_S (dimensionless) is the surface heterogeneity of the adsorbent	42

$$\text{adj-}R^2 = 1 - \frac{\sum_{i=1}^{N}\left(q_{e,\,exp} - q_{e,\,cal}\right)^2}{\sum_{i=1}^{N}\left(q_{e,\,exp} - q_{e,\,mean}\right)^2} \quad (4)$$

$$\text{red-}\chi^2 = \sum_{i=1}^{N}\frac{\left(q_{e,\,exp} - q_{e,\,cal}\right)^2}{q_{e,\,cal}} \quad (5)$$

$q_{e,exp}$ (mg g^{-1}) and $q_{e,cal}$ (mg g^{-1}) are the equilibrium adsorption capacities defined by the experiment and calculated by the model respectively, $q_{e,mean}$ is the average of $q_{e,exp}$ and N represents the number of experimental points.

3. Results and discussion

3.1. Characterization

The FTIR spectra of pharmaceuticals and biochars (native and used adsorbent) are presented in Fig. 1. According to Pattnaik *et al.*,[43] the interval of weak peaks between 3500 and 3800 cm^{-1} (the recorded peak is around 3750 cm^{-1}) is attributed to the O–H stretching vibrations, which can be assigned to the retention of hydroxides and residual water in the biochar. The vibration observed at 1691 cm^{-1} indicates the presence of C=O groups, typically found in ketones, aldehydes, carboxylic acids, and esters.[44] The peak at 1572 cm^{-1} corresponds to C=C stretching vibrations, commonly present in aromatic compounds.[45] The peaks in the range of 1150 to 1032 cm^{-1} (the detected peak is about 1014 cm^{-1}) are associated with C–O stretching vibrations.[46] The peaks observed at 874 cm^{-1} and 762 cm^{-1} reveal alkynes with the C–H bending vibration.[47] The FTIR spectrum after adsorption shows a decrease in band intensity. This reduction attributed to PRM and DIA removal using the prepared PB-500 is probably driven by a physical adsorption mechanism.[45]

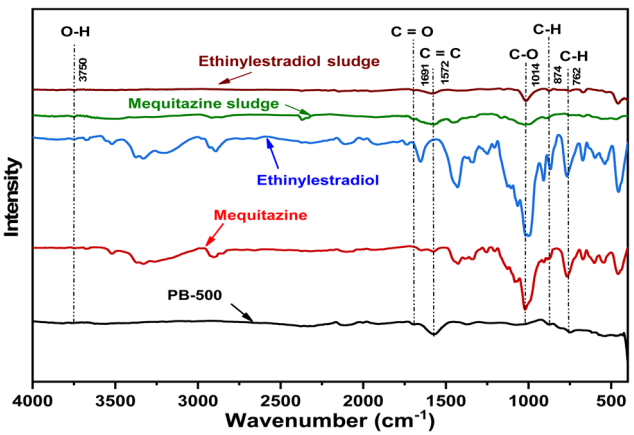

Fig. 1 FTIR spectrum of the native and used biochar.

The scanning electron microscopic (SEM) image results recorded at 50 micrometer resolution before and after adsorption onto PB-500 are presented in Fig. 2. Before adsorption, the biochar exhibits a heterogeneous surface characterized by irregular and high number of pores. After adsorption, the sludge characterization shows changes in the morphology of the biochar. This shift referred to the pore filling mechanism, where implies that the adsorbate molecules have occupied the adsorbent pores and reduced their size.[48] The elemental composition analysis (EDX) of the adsorbent reveals a significant weight percentage of carbon, accounting for 75.35% and 23.1% of oxygen. As depicted in Table 3, adsorption introduces new elements with low concentrations (aluminum, potassium and phosphorus) that were not initially in the prepared biochar. These new elements may derive from the chemical structure of the pharmaceutical compounds. The elements Al, K, and P detected by the EDX analysis in the two active ingredients, mequitazine and ethinylestradiol, could originate from other additives used for encapsulating the medications. These additives are probably associated with the tablet formulation of the drugs Diane and Primalan, respectively.

According to Amalina *et al.*,[49] biochar pores are categorized as micropores (<2 nm), mesopores (2–50 nm) or macropores (>50 nm). In Fig. 3(a), it can be observed that the prepared biochar is mesoporous and exhibits heterogeneous pore size distribution, which was confirmed by nitrogen adsorption/desorption isotherm curves, presented in Fig. 3(b). According

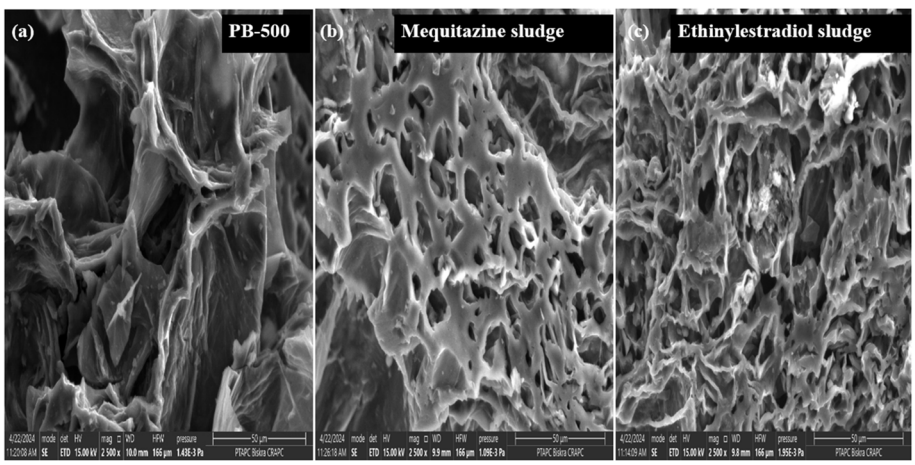

Fig. 2 SEM image of PB-500: (a) before adsorption tests, and (b) and (c) after adsorption of mequitazine and ethinylestradiol, respectively.

Table 3 Elemental composition of the native and used biochar

	Pumpkin adsorbent		Mequitazine sludge		Ethinylestradiol sludge	
	Weight%	Atom%	Weight%	Atom%	Weight%	Atom%
C	75.25	80.97	76.60	81.90	72.43	79.67
O	23.10	18.63	21.68	17.40	21.70	17.92
Mg	0.41	0.22	0.39	0.20	0.96	0.52
Al	—	—	0.38	0.18	0.52	0.26
K	—	—	0.95	0.31	0.89	0.30
P	—	—	—	—	0.99	0.42

Table 4 Physical properties of PB-500

	Unit	Value
S_{BET}	$m^2\ g^{-1}$	8.69
$S_{Micropore}$	$m^2\ g^{-1}$	17.21
V_{Total}	$cm^3\ g^{-1}$	0.01
Average pore diameter	nm	4.79

to the IUPAC nomenclature, the isotherm was categorized as type IV,[50] suggesting that the biochar has mesoporous characteristics. The results showed that the specific area and total volume of pores were 8.69 $m^2\ g^{-1}$ and 0.01 $cm^3\ g^{-1}$ respectively, where the average pore diameter (L_o) was around 4.79 nm. All the properties are listed in Table 4.

The crystalline or amorphous phase composition of the prepared biochar can be deduced through XRD analysis, and the results are presented in Fig. 4(a). The appearance of a broad peak around $2\theta \approx 23°$ indicates the amorphous structure of the biochar, and this peak results from the randomly oriented aromatic carbon structure present in the biochar,[51] while the second peak near $2\theta \approx 42°$ suggests the presence of some graphitic structures or partially ordered carbon. This peak is typically less intense than the first peak, demonstrating the lower degree of order in the graphitic structures.[52]

Fig. 4(b) shows that the pH_{pzc} is around 6.84, which means that the surface of prepared biochar was electrically neutral at this value. The PB-500 was positively charged at pH values less than 6.84 and negatively charged at pH values greater than 6.84.

3.2. Adsorption study

3.2.1. Adsorption kinetic. Fig. 5 illustrates the efficiency removal of mequitazine and ethinylestradiol on PB-500 over a contact time ranging from 0 to 120 min. It appears that the adsorption efficiency increases rapidly at the start until reaching the plateau. The equilibrium time is observed at 30 min for mequitazine and 10 min for ethinylestradiol, where the efficiencies are stabilized at 66.61% and 62.37%, respectively.

Fig. 6(a) and (a′) represent the nonlinear models used, and show the adsorbed quantity q_t (mg g^{-1}) of pharmaceuticals on PB-500 over the same time range (0–120 min). As observed, the adsorbed quantity increases with the increase in contact time until reaching the equilibrium time. The results indicate that the maximum adsorbed quantities are 13.23 mg g^{-1} for mequitazine and 6.24 mg g^{-1} for ethinylestradiol.

Table 5 provides the summary results of both linear and nonlinear models tested. According to the discrepancy between the calculated ($q_{e,cal}$) and the experimental ($q_{e,exp}$) results derived from each model, it can be seen that the PSO provided an adequate description of the experimental data for both mequitazine and ethinylestradiol, with an adj-R^2 value of 0.92 and the lowest red-χ^2 of 0.103. The performance fit of the PSO model suggests that the adsorption of mequitazine and ethinylestradiol onto PB-500 depends on both the adsorbate and the adsorbent,[53] where the rate limiting step is perhaps chemisorption, implicating valence forces through electron sharing or exchange. Similar conclusions were reported in the literature.[54,55]

The intra-particle diffusion model, based on the theory advanced by Weber and Morris,[34] has been widely used for the assessment of adsorption kinetics. If the plot $q_t = f(t^{1/2})$ yields a straight line passing through the origin ($C = 0$), the intra-particle diffusion is considered as the rate-limiting step. When

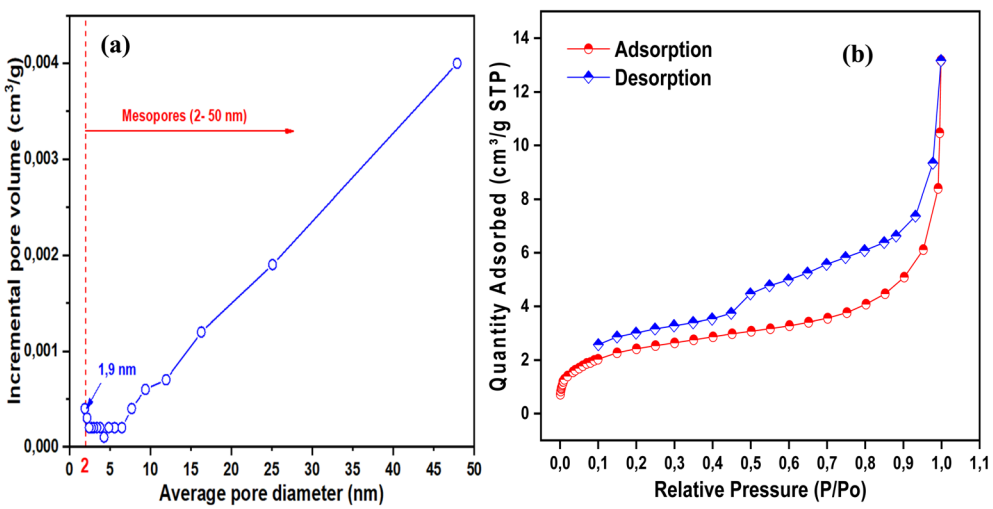

Fig. 3 (a) Pore size distribution of PB-500. (b) Nitrogen adsorption/desorption isotherm of PB-500 at 77 K.

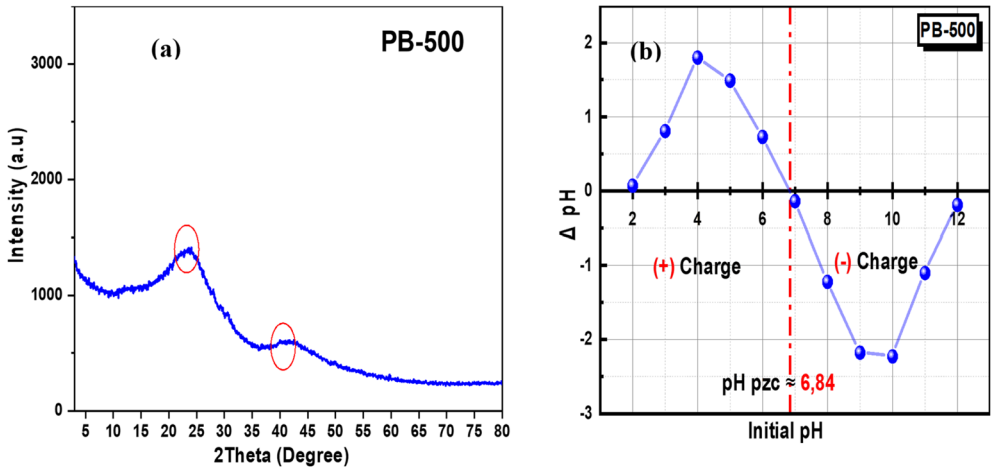

Fig. 4 (a) XRD spectrum and (b) pH at the point of zero charge of PB-500.

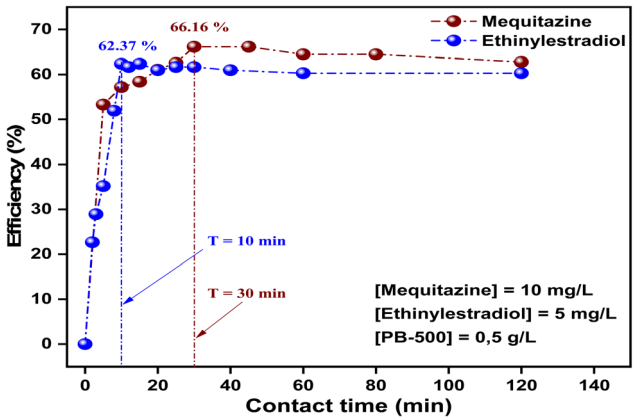

Fig. 5 Adsorption efficiency of mequitazine and ethinylestradiol on the pumpkin biochar as a function of contact time.

$C \neq 0$, both the film and intraparticle diffusion are viewed as rate-limiting steps.[56] The intercept C gives us information on the thickness of the boundary layer, and the larger intercept indicates the greater boundary layer effect.[57] The plot exhibits two distinct steps. The first step corresponds to an external surface adsorption, and the second one reflects gradual adsorption with intra-particle diffusion acting as the rate-limiting step, where the intra-particle diffusion slows down due to the extremely low solute concentration in the solution. The strong correlation of rate data within this model can provide validation for the underlying mechanism.[58] According to this study, the plot (q_t *versus* $t^{1/2}$) presented in Fig. 6(b) and (b′) is bi-linear. From the above-mentioned results, it is observed that $K_{int,1} > K_{int,2}$. The higher value of $K_{int,1}$ reveals that the external diffusion of both mequitazine and ethinylestradiol onto PB-500 was rapid, where the second step corresponds to the internal diffusion and the adsorption attachment.

3.2.2. pH effect. pH effect is a crucial parameter in the adsorption process. The pH of each solution was varied from 2 to 12, knowing that the solutions were modified using either 0.1 M HCl or 0.1 M NaOH. At pH > pH_{pzc} (6.84), the biochar surface was negatively charged. While, at pH < pH_{pzc}, the charge of the PB-500 surface became positive. Fig. 7 shows the medium pH effect, presented by histograms. The results show that the pH change affects the adsorption of pharmaceuticals employed. It is clear that the optimum pH for both pharmaceuticals was around neutrality, what is in agreement with the pK_a value of each pharmaceutical (10.43 for mequitazine and 10.4 for ethinylestradiol).

While studying ethinylestradiol adsorption, Ferandin Honorio *et al.*[59] found that the pH value of 7 notably enhanced the removal, compared to acidic and alkaline media, observing that the adsorbed amount exceeds 0.7 mg g^{-1}. The authors explained that there is an increase in the removal efficiency under alkaline conditions with the increase in the concentration of hydroxyl ions in the solution, resulting in the formation of aqueous complexes that inhibit the adsorption. There are no published data for mequitazine.

3.2.3. Adsorption isotherm. Nonlinear models were applied to well depict the interactions between adsorbate molecules and the adsorbent surface, as shown in Fig. 8, and Langmuir fitting is unable to explain the adsorption mechanism, but it gives us information about the adsorption capacity and the equilibrium process behavior.[60] This model suggests homogeneous adsorption without transmigration or adsorbate interactions on the surface plane.[61] The Freundlich isotherm model is widely used for heterogeneous systems featuring interactions between the adsorbate and the adsorbent.[62] Following the Freundlich theory, the heterogeneity factor n serves as an indicator about the adsorption type. When $n = 1$, the adsorption is linear, when $n < 1$, the adsorption is a favorable and chemical process, but it becomes an unfavorable and physical process when $n > 1$.[63] The Redlich–Peterson model combines both Langmuir and Freundlich models into an integrated equation. At high concentrations, the adsorption shows Freundlich's multilayer behavior. While at lower concentrations, it follows Langmuir's monolayer behavior.[64] The Temkin model explains the effect of indirect interactions between the

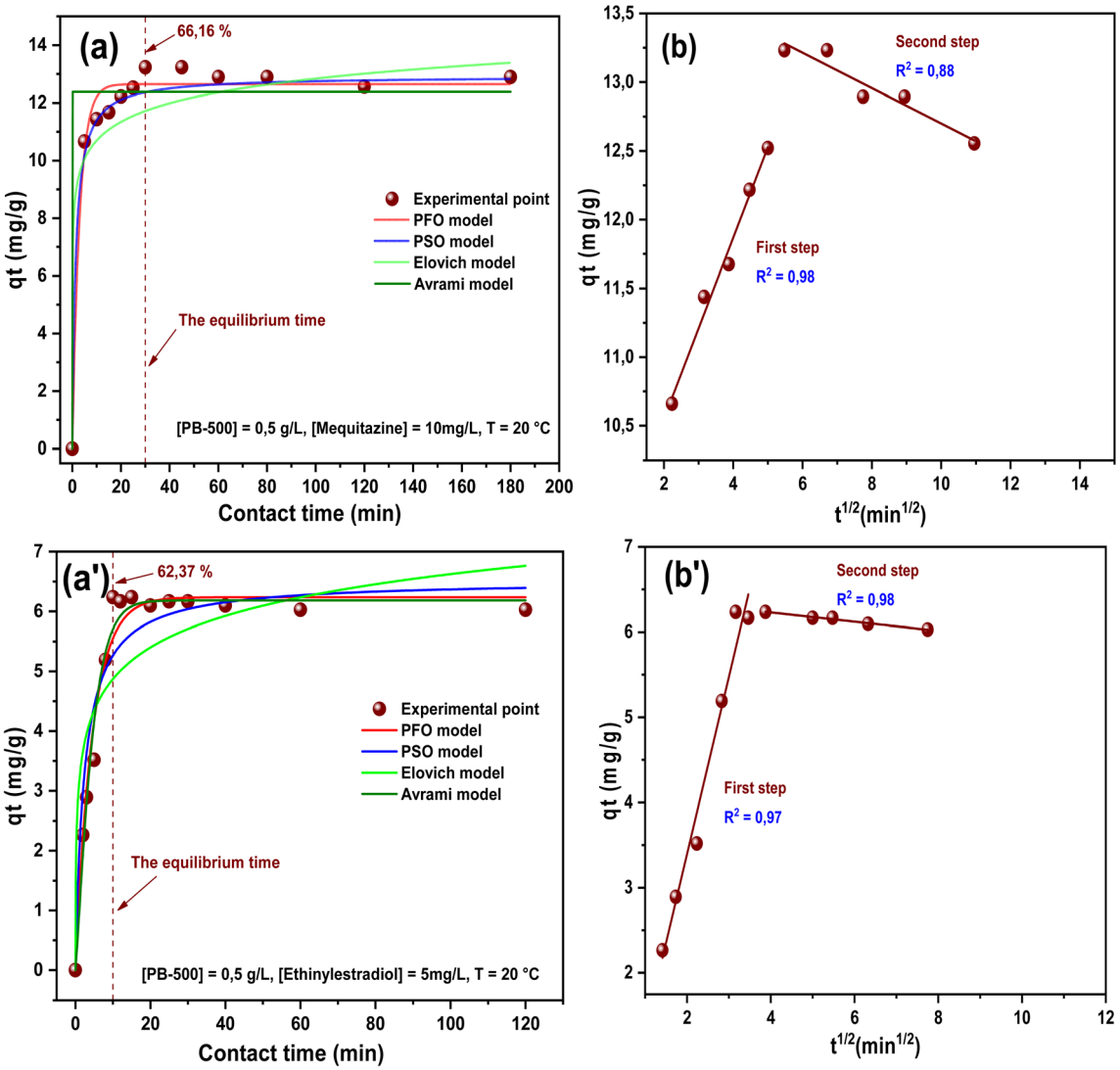

Fig. 6 Kinetic adsorption analysis: (a) and (a′) nonlinear fitting (PFO, PSO, Elovich and Avrami) (b) and (b′) linear intra-particle diffusion fitting.

adsorbent and the adsorbate in the adsorption process. It supposes that as the adsorption capacity increases, the heat energy decreases linearly.[65] The Dubinin–Radushkevich model explains the effect of the porous structure of the adsorbents. It stated that the adsorption process correlated with the filling of micropore volumes, instead of layer-by-layer adsorption on pore walls.[66] The Sips isotherm model is a combination between Langmuir and Freundlich models. At lower concentrations of adsorbate, the Sips isotherm transitions to the Freundlich model and provides a monolayer adsorption capacity similar to the Langmuir isotherm at higher concentrations.[67] The selected parameters of each model are summarized in Table 6. Considering the high (adj-R^2) and lower (red-χ^2) values, the sequence of adsorption isotherms for mequitazine followed the order of Sips > Freundlich > Redlich–Peterson > Langmuir > Temkin > Dubinin–Radushkevich, while the ethinylestradiol isotherm fitting order was Freundlich > Sips > Langmuir > Redlich–Peterson > Temkin > Dubinin–Radushkevich. Regarding the slight difference between the Sips and Freundlich models in terms of adj-R^2 and red-χ^2, it is clear that both the models perform well in describing the adsorption isotherm of mequitazine and ethinylestradiol onto PB-500. The best fitting of the Freundlich model suggests a multilayer adsorption process. It is noteworthy that the Langmuir model achieved the maximum adsorption capacity with 35.6816 mg g^{-1} for mequitazine and 66.2637 mg g^{-1} for ethinylestradiol.

3.2.4. Effect of the PB-500 dosage. The adsorbent dosage effect on mequitazine and ethinylestradiol removal is illustrated in Fig. 9. According to the obtained results, it can be seen that the removal efficiency of both mequitazine and ethinylestradiol was enhanced with the increase in PB-500 doses, until reaching the optimum corresponding to 0.8 g L^{-1} of the adsorbent, where the efficiency achieved 67% for mequitazine and 65.16% for ethinylestradiol. This can be clarified by the increased adsorption active sites.[68] The plateau in efficiency beyond 0.8 g L^{-1} of PB-500 can be explained by multiple factors: particle aggregation at higher dosages reduces the accessible surface area, limits the availability of pharmaceutical molecules

Table 5 Kinetic model parameters for mequitazine and ethinylestradiol adsorption onto PB-500

Model	Unit	Value	
		Mequitazine	Ethinylestradiol
q_e (experiment)	mg g^{-1}	13.23	6.24
PFO			
q_e	mg g^{-1}	12.6449	6.2366
K_1	min^{-1}	0.3344	0.2204
Adj-R^2	—	0.9807	0.9740
Red-χ^2	—	0.2583	0.1014
PSO			
q_e	mg g^{-1}	12.9199	6.5198
K_2	g (mg^{-1} min^{-1})	0.0573	0.0643
Adj-R^2	—	0.9245	0.943
Red-χ^2	—	0.1032	0.0413
Intra-particle diffusion			
$K_{int,1}$	First step mg g^{-1} $min^{-1/2}$	0.6598	2.0804
C_1	mg g^{-1}	9.2289	−0.7658
Adj-R^2	—	0.9806	0.9656
$K_{int,2}$	Second step mg g^{-1} $min^{-1/2}$	−0.1287	−0.0542
C_2	mg g^{-1}	13.9861	6.4475
Adj-R^2	—	0.8862	0.9782
Elovich			
α	mg g^{-1} min^{-1}	8802.2263	45.4329
β	g mg^{-1}	1.0716	1.3125
Adj-R^2	—	0.7626	0.8859
Red-χ^2	—	0.4339	0.1126
Avrami			
q_e	mg g^{-1}	12.3827	6.1830
K_{AV}	min^{-1}	59.4954	0.1624
n_{AV}	—	0.01	1.1963
Adj-R^2	—	0.9447	0.9774
Red-χ^2	—	0.7402	0.0882

to adsorb onto surplus sites, and restricts diffusion in micropores or aggregated particles. These mechanisms provide a clearer understanding beyond saturation alone and are consistent with similar studies in the literature. Our findings align with those of D'Cruz *et al.*[54] and Li *et al.*,[69] which showed that increasing the adsorbent dosage initially enhances promazine and ethinylestradiol removal up to 10 mg and 10 mg L^{-1}, respectively, beyond which the adsorption sites become saturated.

3.2.5. Thermodynamic study. The thermodynamic study aids us to understand the mechanism process of mequitazine and ethinylestradiol adsorption onto the prepared biochar. By investigating the thermodynamic variables such as $\Delta G°$, $\Delta H°$ and $\Delta S°$, which are given as follows:

$$\Delta G^\circ = \Delta H^\circ - T\Delta S^\circ \quad (6)$$

$\Delta G°$ was calculated using the following equation:

$$\Delta G^\circ = -RT\ln(K_C) \quad (7)$$

By replacing eqn (7) into eqn (6) and simplifying, we obtained the following equation:

$$\ln(K_C) = -\frac{\Delta H^\circ}{R} \times \frac{1}{T} + \frac{\Delta S^\circ}{T} \quad (8)$$

where R is the universal gas constant which is equal to 8.314 (J mol^{-1} K^{-1}), T is the absolute temperature and K_C is the thermodynamic equilibrium constant.

K_C was obtained using the following equation:

$$q_e = K_C \times C_e \quad (9)$$

However, $\Delta H°$ and $\Delta S°$ were determined graphically from the linear plot of $\ln(K_C)$ against $(1/T)$ presented in Fig. 10(b) and (b′), as described by Amoo *et al.*[70]

The thermodynamic parameters $\Delta G°$ (kJ mol^{-1}), $\Delta H°$ (kJ mol^{-1}), and $\Delta S°$ (kJ mol^{-1} K^{-1}) represent the Gibbs free energy change, the enthalpy and the entropy change, respectively. The obtained parameter results are presented in Table 7.

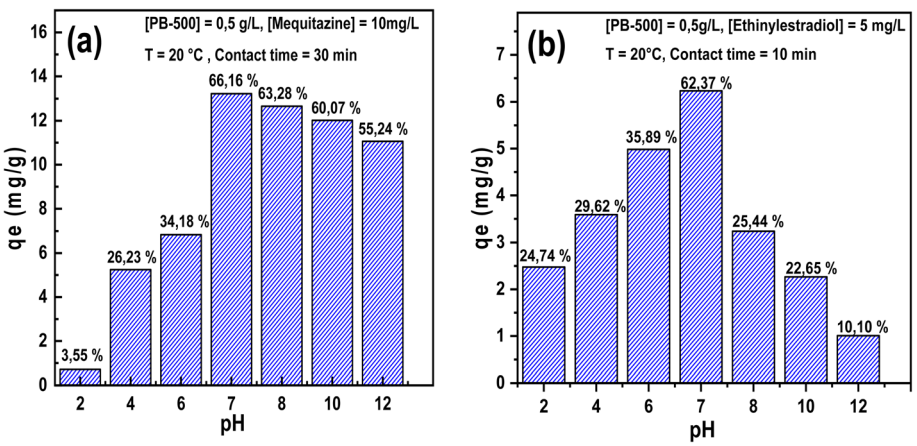

Fig. 7 (a) and (b) pH effect on mequitazine and ethinylestradiol removal.

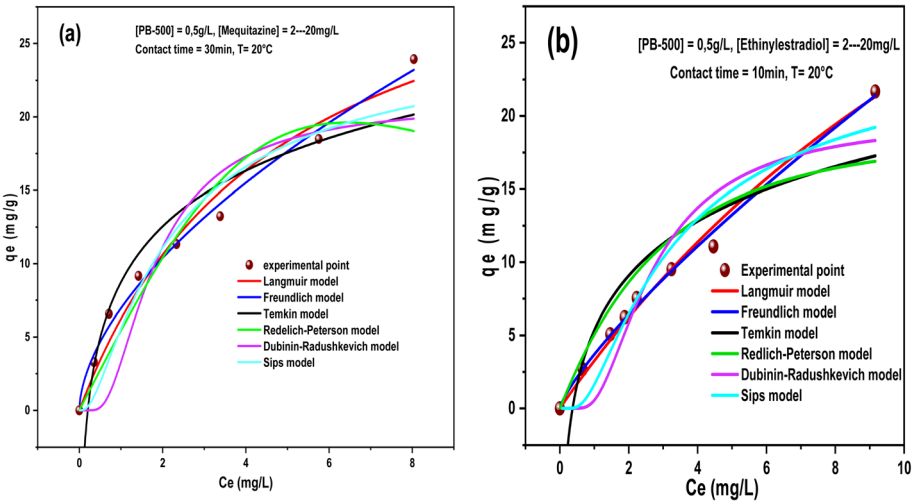

Fig. 8 (a) and (b). Adsorption isotherms of mequitazine and ethinylestradiol onto PB-500.

Table 6 Isotherm modelling parameters for mequitazine and ethinylestradiol adsorption onto PB-500

		Value	
Model	unit	Mequitazine	Ethinylestradiol
Langmuir			
Q_{max}	mg g^{-1}	35.6816	66.2637
K_L	L mg^{-1}	0.2114	0.0518
Adj-R^2	—	0.9691	0.9887
Red-χ^2	—	1.9009	0.4886
Freundlich			
K_F	(mg g^{-1})/(mg L^{-1})^n	6.9586	3.6980
n	—	1.7295	1.2620
Adj-R^2	—	0.9877	0.9924
Red-χ^2	—	0.6144	0.2906
Temkin			
A	mg g^{-1}	5.4863	5.3773
K_T	L g^{-1}	4.9094	2.7062
Adj-R^2	—	0.8776	0.8171
Red-χ^2	—	4.0851	6.2729
Redlich–Peterson			
K_{RP}	(mg L^{-1})$^{-g}$	5.4967	5.8272
α_{RP}	L mg^{-1}	0.0124	0.1531
β	—	2.2406	1.1948
Adj-R^2	—	0.9776	0.9188
Red-χ^2	—	0.9364	2.2735
Dubinin–Radushkevich			
q_m	mg g^{-1}	20.9660	19.8452
β	mol^2 kJ^{-2}	3.8581	7.4296
Adj-R^2	—	0.8673	0.8368
Red-χ^2	—	4.4274	7.0656
Sips			
q_s	mg g^{-1}	26.2452	26.0941
K_S	L mg^{-1}	1.7716	39.5311
n_S	—	3.4719	110.0841
Adj-R^2	—	0.9881	0.9900
Red-χ^2	—	0.4020	0.3713

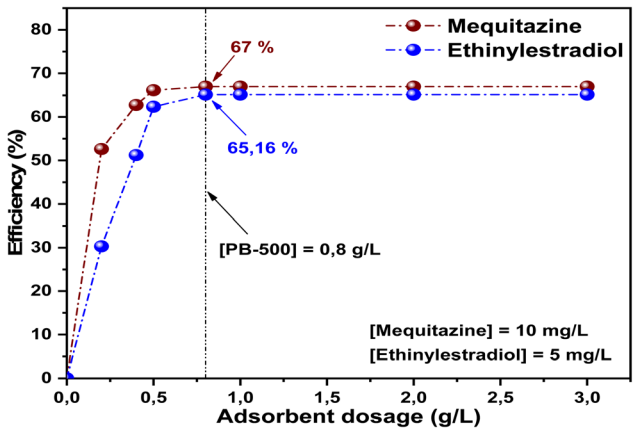

Fig. 9 Effect of the adsorbent dosage on mequitazine and ethinylestradiol removal.

For mequitazine adsorption onto PB-500, it is visible that the free energy was negative at 293 and 313 K and then positive at 323 K. Therefore, the adsorption was favorable and spontaneous until reaching 323 K, signifying that the process becomes non-spontaneous at high temperatures.[71] However, ethinylestradiol adsorption was non-spontaneous and then became spontaneous and favorable at 323 K. The negative value of enthalpy change ΔH° implied the exothermic nature of the adsorption interaction for both pollutants.[72,73] Khumalo *et al.*[74] and Salehi[75] pointed out that the negative values of entropy change ΔS° indicate the decreased disorder in the reaction system for mequitazine and ethinylestradiol. The findings of Ferandin Honorio *et al.*[59] confirmed the same results.

4. Adsorption mechanisms

According to the literature, electrostatic attraction, hydrogen-bonding formation, n–π and π–π interactions, and pore filling are indeed major mechanisms involved in the removal of

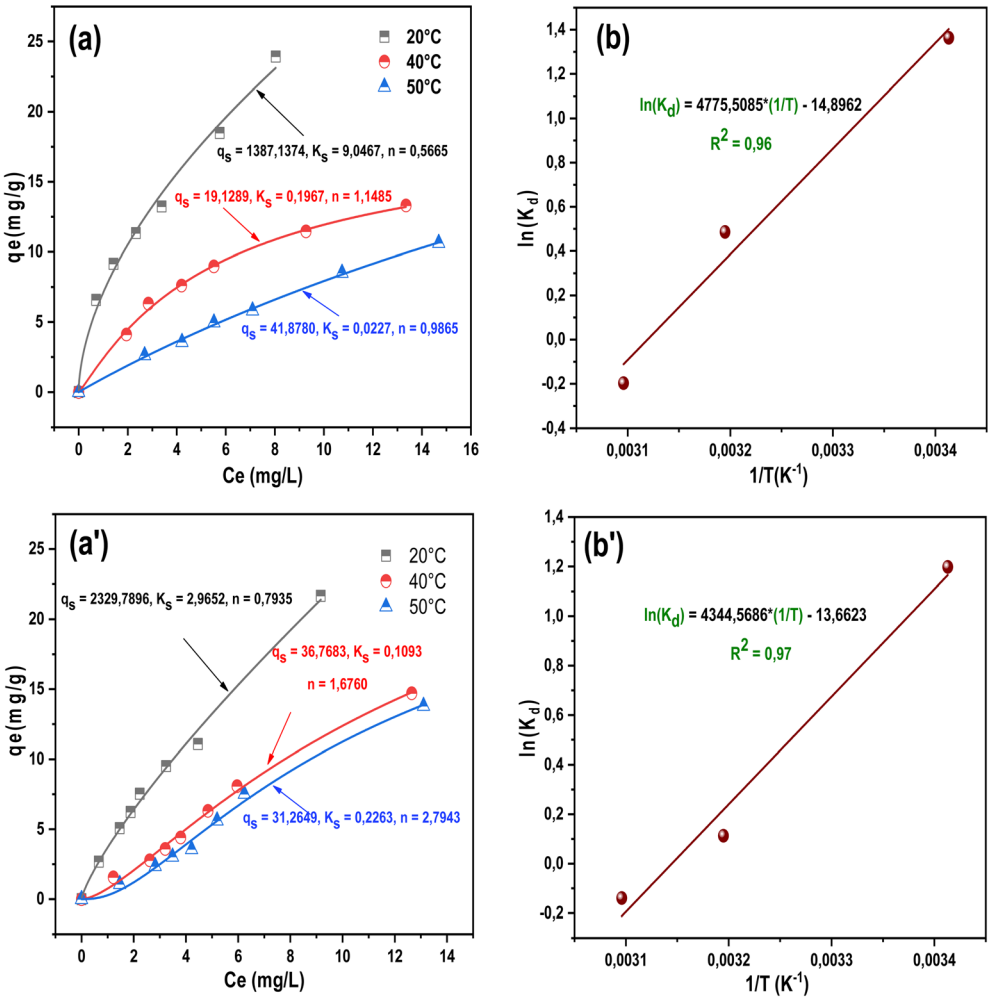

Fig. 10 (a) and (a′) represents the Sips isotherm fitting of mequitazine and ethinylestradiol experimental points at different temperatures (20, 40 and 50 °C). Nonlinear Sips fitting at different temperatures. (b) and (b′) Adsorption thermodynamics graphs at temperatures of 393, 313 and 323 K.

pharmaceuticals from aqueous solutions using porous carbonaceous materials.[27,76–78]

As revealed through the characterization of the biochar before and after adsorption, SEM analysis shows the effect of pore filling mechanism, which is typically associated with physical adsorption.[45] This is supported by FTIR results, which reveal a decrease in the C=C bond intensity, indicating π–π interactions between PB-500 and pollutants.[45] The adsorption kinetics fit well with the pseudo-second-order model, suggesting a contribution of chemical adsorption, where chemisorption involves valence forces or electron exchange.[53] The pH effect further supports the role of physical processes, as the high adsorption efficiency near the pH_{pzc} can be attributed to pore filling or hydrogen bonding mechanisms.[79] Lastly, the best fit with the Freundlich isotherm suggests multilayer adsorption onto a heterogeneous surface dominated by van der Waals forces, hydrogen bonding, and electrostatic interactions.[78]

Based on the obtained results, the adsorption mechanism of mequitazine and ethinylestradiol may involve a combination of physical and chemical processes, where surface interactions and pore filling play a significant role, and possibly additional mechanisms such as valence forces or electron exchange.[80–82]

5. A comparative study with research reported in the literature

Due to the difficulties encountered in obtaining experimental data on the removal of mequitazine and ethinylestradiol in aqueous media through adsorption on biosorbents, we evaluated the effectiveness of our biosorbent (PB-500) in removing these two tested products. To do this, we compared its performance with that of substances having a similar composition to the studied pharmaceuticals, as well as with previous research results on the adsorption of drugs in aqueous solutions using biosorbents/activated adsorbents. Table 8 indicates that under the optimal operating conditions of our bioadsorbent (PB-500), it can serve as an efficient, environmentally friendly, and effective adsorbent for removing pharmaceutical products from aquatic waters.

Table 7 Obtained thermodynamic parameters of mequitazine and ethinylestradiol adsorption onto the pumpkin biochar

				Thermodynamic parameters		
	T (K)	K_d	van't Hoff equation	$\Delta G°$ (kJ mol^{-1})	$\Delta H°$ (kJ mol^{-1})	$\Delta S°$ (J mol^{-1} K^{-1})
Mequitazine	293	3.9100		−3.3216	−39.7036	−123.8470
	313	1.6258	$\ln(K_d) = 4475.5082 \times (1/T) - 14.8962$	−1.2647		
	323	0.8210	$R^2 = 0.96$	0.5296		
Ethinylestradiol	293	3.3148		2.9193	−36.1207	−113.5884
	313	1.1196	$\ln(K_d) = 4344.5686 \times (1/T) - 13.6623$	0.2939		
	323	0.8700	$R^2 = 0.97$	−0.3740		

Table 8 Comparison of mequitazine and ethinylestradiol adsorption capacities in this study with different adsorbents

Adsorbate	Molecular formula	Adsorbent	Efficiency (%)	Adsorption capacity (mg g^{-1})	Q_{max} (mg g^{-1})	Ref
Mequitazine	**$C_{20}H_{22}N_2S$**	**Pumpkin-biochar**	**66.61**	**13.23**	**35.6816**	**Our study**
Promethazine	$C_{17}H_{20}N_2S$	Olive tree pruning biochar	95.87	38.16	346.95	55
Promazine	$C_{17}H_{20}N_2S$	Olive tree pruning biochar	98.64	47.20	640.7	55
Promazine	$C_{17}H_{20}N_2S$	Magnetic activated carbon nanocomposite	99.97	Not given	101.01	54
Ethinylestradiol	**$C_{20}H_{24}O_2$**	**Pumpkin-biochar**	**62.37**	**6.24**	**66.2637**	**Our study**
17α-Ethinylestradiol	$C_{20}H_{24}O_2$	Activated carbon cloths	76	Not given	11.11	76
Ethinylestradiol	$C_{20}H_{24}O_2$	Activated carbon embedded in alginate biopolymer	84	Not given	0.53	77
17α-Ethinylestradiol	$C_{20}H_{24}O_2$	Multi-walled CNTs carbon cryogel	>87.22	5.99	39.22	78
		carbonized hydrothermal carbon	>87.22	5.49	52.90	
			50	0.95	30.75	
Estrone	$C_{18}H_{22}O_2$	Rice husk biomass	86.3	1.82	2.698	59
17β-Estradiol estriol	$C_{18}H_{24}O_2$		94.9	0.69	1.649	
	$C_{18}H_{24}O_3$		82.5	0.22	0.979	

6. Conclusion

Pumpkin peels were investigated to prepare an adsorbent for the removal of mequitazine and ethinylestradiol, which are the activated molecules of Primalan and Diane respectively, from aqueous media. This biosorbent showed promising results for the removal of this type of pollutant. The characterization results indicated that PB-500 was a mesoporous adsorbent characterized by an amorphous structure. Both Sips and Freundlich models demonstrated their performance fitting of the experimental results. The maximum Langmuir adsorption capacity was 35.68 mg g^{-1} for mequitazine and 66.26 mg g^{-1} for ethinylestradiol. The thermodynamic study demonstrated that the adsorption was exothermic with decreased disorder in the reaction system. The findings from the characterization and adsorption experiments demonstrated that the adsorption mechanism is a blend of physical and chemical adsorption. These results indicate that the produced biochar has a remarkable potential for the removal of pharmaceuticals tested.

Data availability

The authors affirm that the data supporting the findings of this study are included in the article. Additional data can be made available from the corresponding author upon reasonable request.

Conflicts of interest

The authors declare that they have no financial conflicts of interest or personal relationships that could have influenced the research findings presented in this study.

Acknowledgements

This work was supported by the Research Laboratory in Subterranean and Surface Hydraulics (LARHYSS) of Mohamed Khider Biskra University (Algeria) and the General Direction of Scientific Research and Technological Development of the Ministry of Higher Education and Scientific Research (Algeria).

References

1 P. Sanga, H. S. Al-mashriqi, J. Chen and H. Qiu, A mechanistic view of removing pharmaceutical-induced pollutants by MXene and MXene-functionalized composites *via* adsorption and advanced oxidation process, *J. Environ. Chem. Eng.*, 2024, **12**(1), 111685.

2 G. Drazdauskaite, J. A. Layhadi and M. H. Shamji, Mechanisms of Allergen Immunotherapy in Allergic Rhinitis, *Curr. Allergy Asthma Rep.*, 2020, **21**(1), 2.

3 J. Kulkarni, Depression as a side effect of the contraceptive pill, *Expert Opin. Drug Saf.*, 2007, **6**(4), 371–374.
4 J. Akhtar, N. A. S. Amin and K. Shahzad, A review on removal of pharmaceuticals from water by adsorption, *Desalin. Water Treat.*, 2015, **57**(27), 12842–12860.
5 J. A. Herrera-Melián, R. Guedes-Alonso, J. C. Tite-Lescano, Z. Sosa-Ferrera and J. J. Santana-Rodríguez, Enhancing pharmaceutical removal in a full-scale constructed wetland with effluent recirculation, *J. Environ. Chem. Eng.*, 2023, **11**(6), 111167.
6 J. Zhang, T. Gao, S. Tang, M. Zheng, M. Wu, J. Wang, B. Lei and L. Tang, Synthesis of novel nitrogen-doped tantalum carbide for pharmaceutical compound adsorption, *J. Environ. Chem. Eng.*, 2024, **12**(2), 112195.
7 J. Rivera-Utrilla, M. Sanchez-Polo, M. A. Ferro-Garcia, G. Prados-Joya and R. Ocampo-Perez, Pharmaceuticals as emerging contaminants and their removal from water. A review, *Chemosphere*, 2013, **93**(7), 1268–1287.
8 J. Cangola, F. K. Abagale and S. J. Cobbina, A systematic review of pharmaceutical and personal care products as emerging contaminants in waters: The panorama of West Africa, *Sci. Total Environ.*, 2024, **911**, 168633.
9 M. Alazaiza, A. Albahnasawi, G. Ali, M. Bashir, D. Nassani, T. Al Maskari, S. Amr and M. Abujazar, Application of Natural Coagulants for Pharmaceutical Removal from Water and Wastewater: A Review, *Water*, 2022, **14**(2), 140.
10 T. Tatarchuk, L. Soltys and W. Macyk, Magnetic adsorbents for removal of pharmaceuticals: A review of adsorption properties, *J. Mol. Liq.*, 2023, **384**, 122174.
11 O. FRAIHA, N. HADOUDI, Z. Najlae, A. SALHI, H. AMHAMDI, F. MOURABIT and M. h. AHARI, Comprehensive Review on the Adsorption of Pharmaceutical Products from Wastewater by Clay Materials, *Desalin. Water Treat.*, 2024, 100114.
12 R. Baccar, M. Sarrà, J. Bouzid, M. Feki and P. Blánquez, Removal of pharmaceutical compounds by activated carbon prepared from agricultural by-product, *Chem. Eng. J.*, 2012, **211–212**, 310–317.
13 K. Samal, S. Mahapatra and M. Hibzur Ali, Pharmaceutical wastewater as Emerging Contaminants (EC): Treatment technologies, impact on environment and human health, *Energy Nexus*, 2022, **6**, 100076.
14 F. Deng, H. Shi, Y. Guo, X. Luo and J. Zhou, Engineering paths of sustainable and green photocatalytic degradation technology for pharmaceuticals and organic contaminants of emerging concern, *Curr. Opin. Green Sustainable Chem.*, 2021, **29**, 100465.
15 J. F. Shaheen, J. O. Eniola and B. Sizirici, Adsorption of ibuprofen from aqueous solution by modified date palm biochar: Performance, optimization, and life cycle assessment, *Bioresour. Technol. Rep.*, 2024, **25**, 101696.
16 J. R. de Andrade, M. F. Oliveira, M. G. C. da Silva and M. G. A. Vieira, Adsorption of Pharmaceuticals from Water and Wastewater Using Nonconventional Low-Cost Materials: A Review, *Ind. Eng. Chem. Res.*, 2018, **57**(9), 3103–3127.
17 V. Calisto, C. I. Ferreira, J. A. Oliveira, M. Otero and V. I. Esteves, Adsorptive removal of pharmaceuticals from water by commercial and waste-based carbons, *J. Environ. Manage.*, 2015, **152**, 83–90.
18 J. O. Osuoha, B. O. Anyanwu and C. Ejileugha, Pharmaceuticals and personal care products as emerging contaminants: Need for combined treatment strategy, *J. Hazard. Mater. Adv.*, 2023, **9**, 100206.
19 Ç. Özer and M. İmamoğlu, Removal of ciprofloxacin from aqueous solutions by pumpkin peel biochar prepared using phosphoric acid, *Biomass Convers. Biorefin.*, 2022, **14**(5), 6521–6531.
20 N. Ghasemi, M. Ahmadi, A. piri, M. Ghasemi and M. Sillanpää, Pb (II) adsorption on pumpkin char and modified pumpkin char: optimisation, kinetics, equilibrium and thermodynamics studies, *Int. J. Environ. Anal. Chem.*, 2020, **102**(14), 3175–3193.
21 S. Chauhan, T. Shafi, B. K. Dubey and S. Chowdhury, Biochar-mediated removal of pharmaceutical compounds from aqueous matrices *via* adsorption, *Waste Dispos. Sustain. Energy*, 2023, **5**(1), 37–62.
22 M. C. Ndoun, H. A. Elliott, H. E. Preisendanz, C. F. Williams, A. Knopf and J. E. Watson, Adsorption of pharmaceuticals from aqueous solutions using biochar derived from cotton gin waste and guayule bagasse, *Biochar*, 2020, **3**(1), 89–104.
23 Z. Kang, X. Jia, Y. Zhang, X. Kang, M. Ge, D. Liu, C. Wang and Z. He, A Review on Application of Biochar in the Removal of Pharmaceutical Pollutants through Adsorption and Persulfate-Based AOPs, *Sustainability*, 2022, **14**(16), 10128.
24 D. Xu, Y. Gao, Z. Lin, W. Gao, H. Zhang, K. Karnowo, X. Hu, H. Sun, S. S. A. Syed-Hassan and S. Zhang, Application of Biochar Derived From Pyrolysis of Waste Fiberboard on Tetracycline Adsorption in Aqueous Solution, *Front. Chem.*, 2019, **7**, 943.
25 Y. Tang, Y. Li, L. Zhan, D. Wu, S. Zhang, R. Pang and B. Xie, Removal of emerging contaminants (bisphenol A and antibiotics) from kitchen wastewater by alkali-modified biochar, *Sci. Total Environ.*, 2022, **805**, 150158.
26 X. Zhu, M. He, Y. Sun, Z. Xu, Z. Wan, D. Hou, D. S. Alessi and D. C. W. Tsang, Insights into the adsorption of pharmaceuticals and personal care products (PPCPs) on biochar and activated carbon with the aid of machine learning, *J. Hazard. Mater.*, 2022, **423**(Pt B), 127060.
27 M. Chebbi, S. Ounoki, L. Youcef and A. Amrane, Synthesis and characterization of pine cones biochar for the removal of an antibiotic (Metronidazole) from aqueous solutions, *J. Ind. Eng. Chem.*, 2023, **126**, 327–339.
28 N. El-Ragehy, A. Badawey and S. El Khateeb, Stability indicating methods for assay of mequitazine in presence of its degradate, *J. Pharm. Biomed. Anal.*, 2002, **29**(1–2), 121–137.
29 L. Meite, R. Szabo, P. Mazellier and J. De Laat, Cinétique de phototransformation de polluants organiques émergents en solution aqueuse diluée, *Rev. Sci. Eau*, 2010, **23**(1), 31–39.
30 J. Wang and X. Guo, Adsorption kinetic models: Physical meanings, applications, and solving methods, *J. Hazard. Mater.*, 2020, **390**, 122156.

31 O. G. Okpara, O. M. Ogbeide, O. C. Ike, K. C. Menechukwu and E. C. Ejike, Optimum isotherm by linear and nonlinear regression methods for lead (II) ions adsorption from aqueous solutions using synthesized coconut shell–activated carbon (SCSAC), *Toxin Rev.*, 2020, **40**(4), 901–914.
32 S. K. Lagergren, About the Theory of So-Called Adsorption of Soluble Substances, *Sven. Vetenskapsakad. Handingarl*, 1898, **24**, 1–39.
33 Y.-S. Ho and G. McKay, Pseudo-second order model for sorption processes, *Process Biochem.*, 1999, **34**(5), 451–465.
34 W. J. Weber Jr and J. C. Morris, Kinetics of adsorption on carbon from solution, *J. Sanit. Eng. Div., Am. Soc. Civ. Eng.*, 1963, **89**(2), 31–59.
35 I. McLintock, The Elovich equation in chemisorption kinetics, *Nature*, 1967, **216**(5121), 1204–1205.
36 M. Avrami, Kinetics of phase change. I General theory, *J. Chem. Phys.*, 1939, **7**(12), 1103–1112.
37 I. Langmuir, The adsorption of gases on plane surfaces of glass, mica and platinum, *J. Am. Chem. Soc.*, 1918, **40**(9), 1361–1403.
38 H. Freundlich, Über die adsorption in lösungen, *Z Phys. Chem.*, 1907, **57**(1), 385–470.
39 R. D. Johnson and F. H. Arnold, The Temkin isotherm describes heterogeneous protein adsorption, *Biochim. Biophys. Acta, Protein Struct. Mol. Enzymol.*, 1995, **1247**(2), 293–297.
40 D. Peterson and O. Redlich, Sorption of Normal Paraffins by Molecular Sieves Type 5A, *J. Chem. Eng. Data*, 1962, **7**(4), 570–574.
41 B. Rand, On the empirical nature of the Dubinin—Radushkevich equation of adsorption, *J. Colloid Interface Sci.*, 1976, **56**(2), 337–346.
42 R. Sips, On the structure of a catalyst surface, *J. Chem. Phys.*, 1948, **16**(5), 490–495.
43 D. Pattnaik; S. Kumar; S. Bhuyan; S. Mishra In Effect of carbonization temperatures on biochar formation of bamboo leaves, *IOP Conference Series: Materials Science and Engineering*, IOP Publishing: 2018; p. 012054.
44 U. Younis, A. A. Rahi, S. Danish, M. A. Ali, N. Ahmed, R. Datta, S. Fahad, J. Holatko, T. Hammerschmiedt and M. Brtnicky, Fourier Transform Infrared Spectroscopy vibrational bands study of Spinacia oleracea and Trigonella corniculata under biochar amendment in naturally contaminated soil, *PLoS One*, 2021, **16**(6), e0253390.
45 N. Rouahna, D. B. Salem, I. Bouchareb, A. Nouioua, A. Ouakouak, A. Fadel, N. Hamdi and R. Boopathy, Reduction of crystal violet dye from water by pomegranate peel–derived efficient biochar: influencing factors and adsorption behaviour, *Water, Air, Soil Pollut.*, 2023, **234**(5), 324.
46 K. Kozłowicz, R. Różyło, B. Gładyszewska, A. Matwijczuk, G. Gładyszewski, D. Chocyk, K. Samborska, J. Piekut and M. Smolewska, Identification of sugars and phenolic compounds in honey powders with the use of GC–MS, FTIR spectroscopy, and X-ray diffraction, *Sci. Rep.*, 2020, **10**(1), 16269.
47 B. A. Armynah, Z. Djafar, W. H. Piarah and D. Tahir, Analysis of chemical and physical properties of biochar from rice husk biomass, *J. Phys.: Conf. Ser.*, 2018, 012038.
48 İ. Küçük, Improvement of methylene blue adsorption properties of lemon peel by surface modification, *Chem. Data Collect.*, 2023, **46**, 101042.
49 F. Amalina, A. S. Abd Razak, S. Krishnan, A. Zularisam and M. Nasrullah, A comprehensive assessment of the method for producing biochar, its characterization, stability, and potential applications in regenerative economic sustainability–a review, *Cleaner Mater.*, 2022, **3**, 100045.
50 K. S. Sing, Reporting physisorption data for gas/solid systems with special reference to the determination of surface area and porosity (Recommendations 1984), *Pure Appl. Chem.*, 1985, **57**(4), 603–619.
51 Y. Liu, X. Zhao, J. Li, D. Ma and R. Han, Characterization of bio-char from pyrolysis of wheat straw and its evaluation on methylene blue adsorption, *Desalin. Water Treat.*, 2012, **46**(1–3), 115–123.
52 F. H. Abdulrazzak; A. F. Alkiam; F. H. Hussein, Behavior of X-ray analysis of carbon nanotubes. *Perspect. Carbon Nanotubes* 2019.
53 V. Vimonses, S. Lei, B. Jin, C. W. K. Chow and C. Saint, Kinetic study and equilibrium isotherm analysis of Congo Red adsorption by clay materials, *Chem. Eng. J.*, 2009, **148**(2–3), 354–364.
54 B. D'Cruz, M. Madkour, M. O. Amin and E. Al-Hetlani, Efficient and recoverable magnetic AC-Fe_3O_4 nanocomposite for rapid removal of promazine from wastewater, *Mater. Chem. Phys.*, 2020, **240**, 122109.
55 M. El-Azazy, A. S. El-Shafie, S. Fawzy, D. W. Rooney and A. I. Osman, Competitive adsorptive removal of promazine and promethazine from wastewater using olive tree pruning biochar: operational parameters, kinetics, and equilibrium investigations, *Environ. Sci. Pollut. Res.*, 2023, **30**(34), 82387–82405.
56 S. Svilović, D. Rušić and A. Bašić, Investigations of different kinetic models of copper ions sorption on zeolite 13X, *Desalination*, 2010, **259**(1–3), 71–75.
57 F.-C. Wu, R.-L. Tseng and R.-S. Juang, Initial behavior of intraparticle diffusion model used in the description of adsorption kinetics, *Chem. Eng. J.*, 2009, **153**(1–3), 1–8.
58 S. Karaca, A. Gurses, M. Ejder and M. Acikyildiz, Kinetic modeling of liquid-phase adsorption of phosphate on dolomite, *J. Colloid Interface Sci.*, 2004, **277**(2), 257–263.
59 J. Ferandin Honorio, M. T. Veit, P. Y. R. Suzaki, P. F. Coldebella, E. Sloboda Rigobello and C. R. G. Tavares, Adsorption of naturals hormones estrone, 17β-estradiol, and estriol by rice husk: monocomponent and multicomponent kinetics and equilibrium, *Environ. Technol.*, 2018, **41**(9), 1075–1092.
60 C. Puri and G. Sumana, Highly effective adsorption of crystal violet dye from contaminated water using graphene oxide intercalated montmorillonite nanocomposite, *Appl. Clay Sci.*, 2018, **166**, 102–112.

61 P. S. Ghosal and A. K. Gupta, Determination of thermodynamic parameters from Langmuir isotherm constant-revisited, *J. Mol. Liq.*, 2017, **225**, 137–146.
62 J. L. Diaz De Tuesta, F. F. Roman, V. C. Marques, A. S. Silva, A. P. F. Silva, T. C. Bosco, A. A. Shinibekova, S. Aknur, M. S. Kalmakhanova, B. K. Massalimova, M. Arrobas, A. M. T. Silva and H. T. Gomes, Performance and modeling of Ni(II) adsorption from low concentrated wastewater on carbon microspheres prepared from tangerine peels by FeCl3-assisted hydrothermal carbonization, *J. Environ. Chem. Eng.*, 2022, **10**(5), 108143.
63 H. N. Tran, S. J. You, A. Hosseini-Bandegharaei and H. P. Chao, Mistakes and inconsistencies regarding adsorption of contaminants from aqueous solutions: A critical review, *Water Res.*, 2017, **120**, 88–116.
64 V. Choudhary, M. Patel, C. U. Jr. Pittman and D. Mohan, Batch and Continuous Fixed-Bed Lead Removal Using Himalayan Pine Needle Biochar: Isotherm and Kinetic Studies, *ACS Omega*, 2020, **5**(27), 16366–16378.
65 N. Ayawei, A. N. Ebelegi and D. Wankasi, Modelling and Interpretation of Adsorption Isotherms, *J. Chem.*, 2017, **2017**, 1–11.
66 Q. Hu and Z. Zhang, Application of Dubinin–Radushkevich isotherm model at the solid/solution interface: A theoretical analysis, *J. Mol. Liq.*, 2019, **277**, 646–648.
67 K. Y. Foo and B. H. Hameed, Insights into the modeling of adsorption isotherm systems, *Chem. Eng. J.*, 2010, **156**(1), 2–10.
68 C. Rudram, P. Dinesh Sankar Reddy and S. K. Kuruva, Fluoride removal from aqueous solution using thermally treated dolomite powder as adsorbent, *Mater. Today: Proc.*, 2024, **13**, 1.
69 Q. Li, X. Ma, N. Gao and W. Chu, Removal of 17α-ethynylestradiol from aqueous solutions by a hybrid PAC/UF process, *Water Sanit.*, 2017, **43**(1), 116–121.
70 K. O. Amoo, T. E. Amoo, O. A. Olafadehan, E. E. Alagbe, A. J. Adesina, M. O. Bamigboye, B. D. Olowookere and K. D. Ajayi, Adsorption of cobalt (II) ions from aqueous solution using cow bone and its derivatives: Kinetics, equilibrium and thermodynamic comparative studies, *Results Eng.*, 2023, **20**, 101635.
71 A. Toptas, S. Demierege, E. Mavioglu Ayan and J. Yanik, Spent Mushroom Compost as Biosorbent for Dye Biosorption, *Clean:Soil, Air, Water*, 2014, **42**(12), 1721–1728.
72 H. Atlas, M. Sadoq, S. Imame, A. Amar, A. Kali, I. Loulidi, F. Z. Mamouni, M. Jabri, H. Chaimaa, M. N. Bennani, A. Palsan Sannasi and F. Boukhlifi, Sustainable biosorption of Methylthioninium Chloride in wastewaters using new Cystoseira barbata seaweed: Equilibrium isotherm, kinetic modeling and mechanism analysis, *Arabian J. Chem.*, 2024, **17**(2), 101635.
73 T. Handayani, D. Emriadi, P. Ramadhani and R. Zein, Modelling studies of methylene blue dye removal using activated corn husk waste: Isotherm, kinetic and thermodynamic evaluation, *S. Afr. J. Chem. Eng.*, 2024, **47**, 15–27.
74 S. M. Khumalo, B. F. Bakare and S. Rathilal, Single and multicomponent adsorption of amoxicillin, ciprofloxacin, and sulfamethoxazole on chitosan-carbon nanotubes hydrogel beads from aqueous solutions: Kinetics, isotherms, and thermodynamic parameters, *J. Hazard. Mater. Adv.*, 2024, **13**, 100404.
75 M. Salehi, Evaluating the industrial potential of naturally occurring proteases: A focus on kinetic and thermodynamic parameters, *Int. J. Biol. Macromol.*, 2024, **254**(Pt 2), 127782.
76 R. Ghorbali, L. Sellaoui, H. Ghalla, A. Bonilla-Petriciolet, R. Trejo-Valencia, A. Sánchez-Barroso, S. Deng and A. B. Lamine, In-depth study of adsorption mechanisms and interactions in the removal of pharmaceutical contaminants *via* activated carbon: a physicochemical analysis, *Environ. Sci. Pollut. Res.*, 2024, 1–9.
77 T. Hubetska, N. Kobylinska and J. R. García, Efficient adsorption of pharmaceutical drugs from aqueous solution using a mesoporous activated carbon, *Adsorption*, 2020, **26**(2), 251–266.
78 M. E. Peñafiel and D. Flores, Competitive adsorption of drugs from a multi-component mixture on sugarcane bagasse, *Water*, 2023, **15**(11), 2127.
79 H. N. Tran, Y.-F. Wang, S.-J. You and H.-P. Chao, Insights into the mechanism of cationic dye adsorption on activated charcoal: The importance of π–π interactions, *Process Saf. Environ. Prot.*, 2017, **107**, 168–180.
80 D. Prokić, M. Vukčević, A. Kalijadis, M. Maletić, B. Babić and T. Đurkić, Removal of Estrone, 17β-Estradiol, and 17α-Ethinylestradiol from Water by Adsorption onto Chemically Modified Activated Carbon Cloths, *Fibers Polym.*, 2020, **21**(10), 2263–2274.
81 S. A. Abdel-Gawad and H. M. Abdel-Aziz, Removal of ethinylestradiol by adsorption process from aqueous solutions using entrapped activated carbon in alginate biopolymer: isotherm and statistical studies, *Appl. Water Sci.*, 2019, **9**, 75.
82 D. Prokić, M. Vukčević, A. Mitrović, M. Maletić, A. Kalijadis, I. Janković-Častvan and T. Đurkić, Adsorption of estrone, 17β-estradiol, and 17α-ethinylestradiol from water onto modified multi-walled carbon nanotubes, carbon cryogel, and carbonized hydrothermal carbon, *Environ. Sci. Pollut. Res.*, 2021, **29**(3), 4431–4445.